Photoluminescence study on polar nanoregions and structural variations in $Pb(Mg_{1/3}Nb_{2/3})O_3$-$PbTiO_3$ single crystals

X. L. Zhang,[1] J. J. Zhu,[1] J. Z. Zhang, [1] G. S. Xu,[2] Z. G. Hu,[1,*] and J. H. Chu [1]

[1]*Key Laboratory of Polar Materials and Devices, Ministry of Education, Department of Electronic Engineering, East China Normal University, Shanghai 200241, China*
[2]*R&D Center of Synthetic Crystals, Shanghai Institute of Ceramics, Chinese Academy of Sciences, Shanghai 201800, China*

[*]*zghu@ee.ecnu.edu.cn*

Abstract: We report polar nanostructure and electronic transitions in relaxor ferroelectric $Pb(Mg_{1/3}Nb_{2/3})O_3$-$PbTiO_3$ (PMN-PT) single crystals around morphotropic phase boundary (MPB) region by variable-temperature (80-800 K) photoluminescence (PL) spectra and low-wavenumber Raman scattering (LWRS). The discontinuous evolution from peak positions and intensity of luminescence emissions can be corresponding to formation of polar nanoclusters and phase transitions. Six emissions have been derived from PL spectra and show obvious characteristics near phase transition temperatures, which indicates that PL spectral measurement is promising in understanding the microcosmic mechanism. The Raman mode at 1145 cm^{-1} indicates that temperature dependent luminescence phenomena can be modulated by thermal quenching.

OCIS codes: (240.0240) Optics at surfaces; (160.4760) Optical properties; (130.2260) Ferroelectrics.

References and links

1. S.-E. Park and T. R. Shrout, "Ultrahigh strain and piezoelectric behavior in relaxor based ferroelectric single crystals," J. Appl. Phys. **82**, 1804–1811 (1997).
2. S. Kamba and J. Petzelt, in *Piezoelectric Single Crystals and Their Application*, S. Trolier-McKinstry, L. E. Cross and Y. Yamashita, eds. (Penn State University, Penn State, 2004).
3. A. S. Mischenko, Q. Zhang, R. W. Whatmore, J. F. Scott, and N. D. Mathur, "Giant electrocaloric effect in the thin film relaxor ferroelectric $0.9Pb(Mg_{1/3}Nb_{2/3})O_3$-$0.1PbTiO_3$ near room temperature," Appl. Phys. Lett. **89**, 242912 (2006).
4. J. F. Scott, "Applications of modern ferroelectrics," Science **315**, 954–959 (2007).
5. M. Suewattana and D. J. Singh, "Electronic structure and lattice distortions in $PbMg_{1/3}Nb_{2/3}O_3$ studied with density functional theory using the linearized augmented plane-wave method," Phys. Rev. B **73**, 224105 (2006).
6. B. Mihailova, B. Maier, C. Paulmann, T. Malcherek, J. Ihringer, M. Gospodinov, R. Stosch, B. Güttler, and U. Bismayer, "High-temperature structural transformations in the relaxor ferroelectrics $PbSc_{0.5}Ta_{0.5}O_3$ and $Pb_{0.78}Ba_{0.22}Sc_{0.5}Ta_{0.5}O_3$," Phys. Rev. B **77**, 174106 (2008).
7. S. F. Liu, S. E. Park, T. R. Shrout, and L. E. Cross, "Electric field dependence of piezoelectric properties for rhombohedral $0.955Pb(Zn_{1/3}Nb_{2/3})O_3$-$0.045PbTiO_3$ single crystals," J. Appl. Phys. **85**, 2810–2814 (1999).

#212614 - $15.00 USD Received 23 May 2014; revised 18 Aug 2014; accepted 19 Aug 2014; published 2 Sep 2014

8. M. Ahart, M. Somayazulu, R. E. Cohen, P. Ganesh, P. Dera, H.-k. Mao, R. J. Hemley, Y. Ren, P. Liermann, and Z. G. Wu, "Origin of morphotropic phase boundaries in ferroelectrics," *Nature* **451**, 545–548 (2008).
9. H. X. Fu and R. E. Cohen, "Polarization rotation mechanism for ultrahigh electromechanical response in single-crystal piezoelectrics," *Nature* **403**, 281–283 (2000).
10. B. Noheda, D. E. Cox, G. Shirane, S.-E. Park, L. E. Cross, and Z. Zhong, "Polarization Rotation via a Monoclinic Phase in the Piezoelectric $0.92PbZn_{1/3}Nb_{2/3}O_3$-$0.08PbTiO_3$," Phys. Rev. Lett. **86**, 3891–3894 (2001).
11. R. Kesavamoorthy and V. Sivasubramanian, "Core-shell nanostructure and its phase transitions in $Pb(Mg_{1/3}Nb_{2/3})O_3$ by Raman spectroscopy and photoluminescence," J. Raman Spectrosc. **38**, 762–769 (2007).
12. H. Takenaka, I. Grinberg, and A. M. Rappe, "Anisotropic Local Correlations and Dynamics in a Relaxor Ferroelectric," Phys. Rev. Lett. **110**, 147602 (2013).
13. D. A. Viehland, S. J. Jang, L. E. Cross, and M. Wuttig, "Freezing of the polarization fluctuations in lead magnesium niobate relaxors," J. Appl. Phys. **68**, 2916–2921 (1990).
14. A. Dejneka, I. Aulika, V. Trepakov, J. Krepelka, L Jastrabik, denek Hubicka, and A. Lynnyk, "Spectroscopic ellipsometry applied to phase transitions in solids: possibilities and limitations," Opt. Express **17**, 14322–14338 (2009).
15. X. L. Zhang, Z. G. Hu, G. S. Xu, J. J. Zhu, Y. W. Li, Z. Q. Zhu, and J. H. Chu, "Optical bandgap and phase transition in relaxor ferroelectric $Pb(Mg_{1/3}Nb_{2/3})O_3$-$xPbTiO_3$ single crystals: An inherent relationship," Appl. Phys. Lett. **103**, 051902 (2013).
16. J. J. Zhu, K. Jiang, G. S. Xu, Z. G. Hu, Y. W. Li, Z. Q. Zhu, and J. H. Chu, "Temperature-dependent Raman scattering and multiple phase coexistence in relaxor ferroelectric $Pb(In_{1/2}Nb_{1/2})O_3$-$Pb(Mg_{1/3}Nb_{2/3})O_3$-$PbTiO_3$ single crystals," J. Appl. Phys. **114**, 153508 (2013).
17. X. Chen, P. P Jiang, Z. H. Duan, Z. G. Hu, X. F. Chen, G. S. Wang, X. L. Dong, and J. H. Chu, "The A-site driven phase transition procedure of $(Pb_{0.97}La_{0.02})(Zr_{0.42}Sn_{0.40}Ti0.18)O_3$ ceramics: An evidence from electronic structure variation," Appl. Phys. Lett. **103**, 192910 (2013).
18. H. Idink and W. B. White, "Raman spectroscopic study of order-disorder in lead magnesium niobate," J. Appl. Phys. **76**, 1789–1793 (1994).
19. H. Ohwa, M. Iwata, H. Orihara, N. Yasuda, and Y. Ishibashi, "Raman Scattering in (1-x)$Pb(Mg_{1/3}Nb_{2/3})O_3$-$xPbTiO_3$," J. Phys. Soc. Jpn. **70**, 3149–3154 (2001).
20. F. J. Meng, Z.-Y. Cheng, B. K. Rai, R. S. Katiyar, E. Alberta, R. Guo, and A. S. Bhalla, "Photoluminescence in $PbMg_{1/3}Nb_{2/3}O_3$-$PbIn_{1/2}Nb_{1/2}O_3$ systems," J. Mater. Res. **13**, 1861–1864 (1998).
21. P. Zhang, M. Shen, L. Fang, F. Zheng, X. Wu, J. Shen, and H. Chen, "Pr^{3+} photoluminescence in ferroelectric $(Ba_{0.77}Ca_{0.23})TiO_3$ ceramics: Sensitive to polarization and phase transitions," Appl. Phys. Lett. **92**, 222908 (2008).
22. J. H. Rho, S. H. Jang, Y. D. Ko, S. J. Kang, D.-W. Kim, J.-S. Chung, M. Kim, M. Han, and E. Choi, "Photoluminescence induced by thermal annealing in SrTiO3 thin film," Appl. Phys. Lett. **95**, 241906 (2009).
23. G. S. Xu, K. Chen, D. F. Yang, and J. B. Li, "Growth and electrical properties of large size $Pb(In_{1/2}Nb_{1/2})O_3$-$Pb(Mg_{1/3}Nb_{2/3})O_3$-$PbTiO_3$ crystals prepared by the vertical Bridgman technique," Appl. Phys. Lett. **90**, 032901 (2007).
24. Y. Y. Liao, Y. W. Li, Z. G. Hu, and J. H. Chu, "Temperature dependent phonon Raman scattering of highly a-axis oriented $CoFe_2O_4$ inverse spinel ferromagnetic films grown by pulsed laser deposition," Appl. Phys. Lett. **100**, 071905 (2012).
25. X. Chen, Z. G. Hu, Z. H. Duan, X. F. Chen, G. S. Wang, X. L. Dong, and J. H. Chu, "Effects from A-site substitution on morphotropic phase boundary and phonon modes of $(Pb_{1-1.5x}La_x)(Zr_{0.42}Sn_{0.40}Ti_{0.18})O_3$ ceramics by temperature dependent Raman spectroscopy," J. Appl. Phys. **114**, 043507 (2013).
26. S. R. Bairavarasu, M. E. Edwards, M. D. Sastry, F. Kochary, P. Kommidi, B. R. Reddy, D. Lianos, and M. D. Aggarwal, "Photomagnetism and photoluminescence (PL) of (Pb-Fe-e^-) complex in lead magnesium niobate-lead titanate (PMN-PT) crystals containing β-PbO nanoclusters ," Spectrochim. Acta, Part A **71**, 1581–1587 (2008).
27. G. Blasse, "Luminescence of lithium niobate ($LiNb_3O_8$)," Phys. State Sol-A. Appl. Res. **20**, K99–K102 (1973).
28. D. P. Volanti, L. S. Cavalcante, E. C. Paris, A. Z. Simões, D. Keyson, V. M. Longo, A. T. de Figueiredo, E. Longo, and J. A. Varela, "Photoluminescent behavior of $SrBi_2Nb_2O_9$ powders explained by means of β-Bi_2O_3 phase," Appl. Phys. Lett. **90**, 261913 (2007).
29. E. Duval, A. Boukenter, and B. Champagnon, "Vibration Eigenmodes and Size of Microcrystallites in Glass: Observation by Very-Low-Frequency Raman Scattering," Phys. Rev. Lett. **56**, 2052–2055 (1986).
30. W. Dmowski, S. B. Vakhrushev, I.-K. Jeong, M. P. Hehlen, F. Trouw, and T. Egami, "Local Lattice Dynamics and the Origin of the Relaxor Ferroelectric Behavior," Phys. Rev. Lett. **100**, 137602 (2008).
31. R. Farhi, M. Marssi, A. Simon, and R. Ravez, "Relaxor-like and spectroscopic properties of niobium modified barium titanate ," Eur. Phys. J. B **18**, 605–610 (2000).
32. S. Shionoya, in *Luminescence of Solids*, D. R. Vij ed. (Plenum Press, New York, 1998).

#212614 - $15.00 USD Received 23 May 2014; revised 18 Aug 2014; accepted 19 Aug 2014; published 2 Sep 2014

1. Introduction

Relaxor ferroelectrics have been a focus of intense attention in recent years because they possess a strong piezoelectric effect, a high permittivity over a broad temperature range, and unique dielectric response with strong frequency dispersion. These materials can be applied in tunable capacitors, actuators, and electro-optic devices [1–6]. As one of the representatives, $Pb(Mg_{1/3}Nb_{2/3})O_3$-$PbTiO_3$ (PMN-PT) single crystal has a high dielectric permittivity and attracts intensive research [7]. It occupies a variety of structures with various compositions and temperatures [8–10]. Initially, excellent dielectric permittivities are attributed to the compositional fluctuations throughout the material. The fluctuation phenomena lead to the existence of small micro-regions with different compositions. Therefore, a distribution of local ferroelectric transition temperatures (Curie temperature, T_c) is responsible for the broad diffuse phase transitions [11]. These micro-regions are discovered as polar nanoregions (PNRs), which form spherical or elliptic clusters in a nonpolar matrix at Burns temperature (T_b). Their sizes can increase due to interactions of the PNRs on cooling until the Vogel-Fulcher freezing temperature (T_f) [12]. The dielectric response of relaxor ferroelectric materials was viewed as the relaxation of these polar clusters over a wide temperature and frequency range. The relaxation dynamics of polar clusters reveal a non-Arrhenius behavior [13]. Recently, intense optical measurements have been carried out to understand structural transitions at low temperatures for PMN-PT and its related system, e.g., transmittance spectra, spectroscopic ellipsometry and Raman scattering [14–17]. These techniques are nondestructive and efficient ways to detect phase transitions. However, nanosized clusters, which lead to the broadening peaks from spectral measurements, especially from Raman scattering, become an obstacle to detect phase transitions. Moreover, the fraction of such clusters is so low that *x*-ray diffraction (XRD) is also difficult to detect them [18, 19]. It is natural to ask how to avoid the effects from nanostructures in distinguishing phase transitions for the above spectra. Therefore, a desired technique, which is sensitive to both evolution of nanostructures and phase transitions, is urgent as an aid for the above spectral measurements.

Following the above considerations, temperature dependence of photoluminescence (PL) spectra and low-wavenumber Raman scattering (LWRS) for PMN-0.24PT and PMN-0.33PT single crystals have been carried out. PL measurement is a common means in understanding band-band excitations. In recent years, it appears to be a reliable experimental technique to probe phase transitions in materials and also sensitive to the evolution of polar nanoclusters [11, 20–22]. Unfortunately, there are few reports on PL spectra of PMN-PT single crystals, especially near morphotropic phase boundary (MPB). The unique advantage makes PL desirable, not only for potential application in optoelectronic devices, but also to answer basic questions on relationship between microcosmic mechanism and macroscopical phenomena in relaxor ferroelectric crystals. Moreover, with mutual verification of these optical measurement, a complete judgement will be established and applied in depth understanding of ferroelectric oxides by a nondestructive way.

In this Letter, temperature dependent intensities and positions of PL spectra for PMN-PT crystals have been observed. We demonstrate that these phenomena can be readily accounted for ferroelectric order. Moreover, the LWRS modes indicate a hypothesis of the cores-hell nanostructure with a 1 : 1 ordered negatively charged nanocore surrounded by a positively charged nanoshell.

2. Experimental

The PMN-*x*PT single crystals were prepared using a vertical Bridgman technique with the PT compositions of x=0.24 and 0.33. The samples are cut perpendicular along the <001> direction [23]. PL spectra were carried out by a Jobin-Yvon LabRAM HR 800 UV spectrometer with a

#212614 - $15.00 USD Received 23 May 2014; revised 18 Aug 2014; accepted 19 Aug 2014; published 2 Sep 2014

He-Cd laser as the excited light, which is operated at the wavelength of 325 nm (3.82 eV). Low-wavenumber Raman scattering (LWRS) were recorded with the same spectrometer using a 633 nm line of a He-Ne laser as the exciting source. The scattering data were recorded from 80 to 600 K by a Linkam THMSE 600 heating/cooling stage with the set-point stability of better than 1 K. The laser beam was focused through a 50× microscope with a working distance of 18 mm. An air-cooled charge coupled device (CCD) (-70 °C) with a 1024×256 pixels front illuminated chip was used to collect the scattered signal dispersed on 1800 grooves/mm grating [24, 25]. Note that no mathematical smoothing has been performed on the experimental data. Peaks of the bare spectra are assigned by using the supporting software NGSLabSpec designed by Jobin-Yvon. The Gauss-Lorentz fitting is applied for further analysis. The expression can be written as:

$$y = a\{g\exp[\frac{-(x-p)^2}{w^2}] + (1-g)/[1+\frac{4(x-p)^2}{w^2}]\}. \quad (1)$$

Here, x and y are the coordinates of fitting points. a, g, p, and w are the fitting parameters.

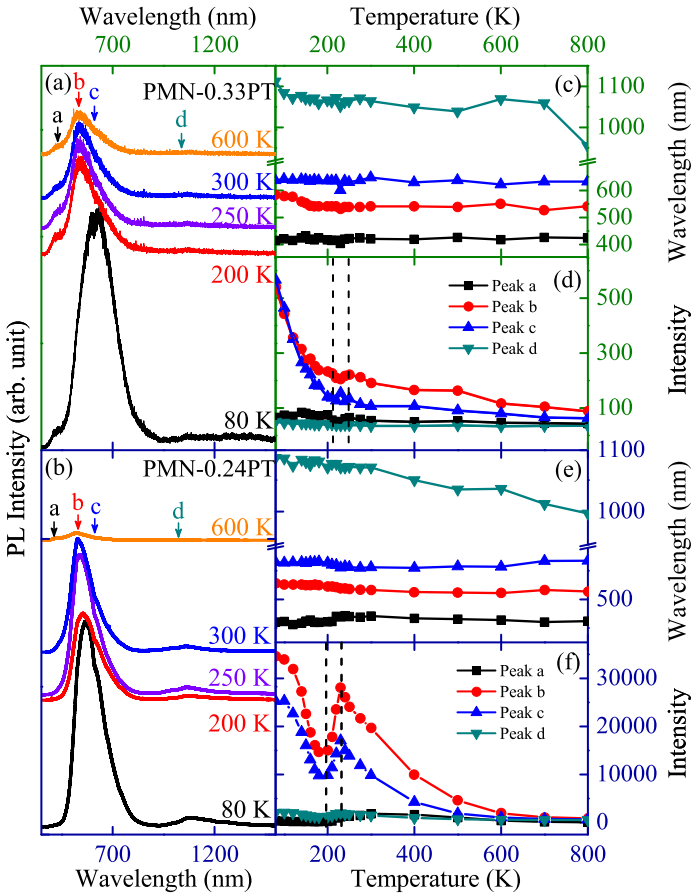

Fig. 1. Temperature dependence of PL spectra for (a) PMN-0.33PT and (b) PMN-0.24PT crystals, respectively. Temperature dependence for peak positions and intensity of (c), (d) PMN-0.33PT and (e), (f) PMN-0.24PT crystals, respectively.

#212614 - $15.00 USD Received 23 May 2014; revised 18 Aug 2014; accepted 19 Aug 2014; published 2 Sep 2014

3. Experimental results

3.1. Variations of position and intensity of bare PL spectra with temperature

Figure 1 shows the PL spectra of PMN-0.24PT and PMN-0.33PT crystals from 350 nm to 1500 nm (0.83-3.55 eV) in the temperature range of 80-600 K. Four peaks (a, b, c, and d) can be observed. The variations of positions and intensities with temperature for all bands are shown in Fig. 1(c)–1(f), respectively. In PL spectroscopy, the photon emitted upon recombination corresponds to transitions between the valence and conduction bands or other interbands in bandgap, which is hence lower than the bandgap. The emission at 425 nm (peak a) can be ascribed to the bandgap energy [15]. It takes a positive trend with temperature which indicates a negative band gap narrowing trend. This negative band gap narrowing trend is usually explained by two factors: thermal expansion of the lattice, and renormalization of the band structure by electron-phonon interaction. The strongest PL emission around 510 nm overlaps with the absorption maximum detected by transmittance spectral measurement [15]. It suggests that the excitation with energy larger than the bandgap creates electron-hole pairs, which get trapped at states in bandgap leaving such centers in electronically excited state. These pairs produce strong PL emissions as they converted into the ground state [26]. As can be seen in Fig. 1(a) and 1(b), the peaks are quite sharp at low temperature and become broadening with increasing temperature. At the same time, the peak intensity of PMN-0.33PT keeps decreasing with increasing temperature, as shown in Fig. 1(d). However, in Fig. 1(f), the peak intensity of PMN-0.24PT takes a decreasing trend below 200 K, upon 230 K and an increasing trend between 200 K and 230 K. The phase transition at T_c ($\sim$250 K) of PMN-0.24PT leads to the abnormal phenomena. Abnormal trend between 200 K and 230 K indicates an intermediate phase (Monoclinic). Note that the PL peak of PMN-0.33PT does not present such significantly abnormal trend. As we know, PL spectra can be related to local polar structures with different symmetry. These peaks are activated by the broken translational symmetry. The intensity is connected with the size of polar nanoclusters and dynamic interactions with local random fields. The PMN-0.33PT, which is near MPB region, is not conducive to produce large polar nanoclusters, while these clusters are more likely to appear in PMN-0.24PT, where only pure phase exists. Therefore, we can see apparent changing process of polar nanoclusters for PMN-0.24PT. The slightly abnormal trend in temperature from 200 to 230 K for PMN-0.33PT comes from the transition from monoclinic phase to tetragonal phase [15]. Niobium (Nb) ion in PMN-PT is responsible for the formation of polar nanoclusters [20] and NbO_6 octahedron is the luminescent center in the perovskitelike niobates [27, 28]. It suggests that the disappearance of the significant temperature dependence from peaks b and c can be attributed to the Nb site centers, which lead to either the growing and merging of polar clusters or the structural phase transition in the material. Position of peak d consists well with the energy from oxygen vacancies to conduct band. Also its behaviors are very similar to oxygen defects, which can induce photoluminescence emission. So we can determine that peak d is caused by oxygen defects. As we know, there is a few defects in single crystals. This is why peak d is so weak and does not behave significant abnormal behavior, as compared to other peaks.

3.2. Nanocluster exiting in PMN-PT confirmed by LWRS

Figure 2 shows the Stokes and anti-Stokes Raman spectra in the low-wavenumber range from -25 to 25 cm^{-1} for PMN-0.24PT and PMN-0.33PT crystals. The Stokes spectra show one peak (20 cm^{-1}) for PMN-0.24PT and three peaks (14, 17, and 19 cm^{-1}) for PMN-0.33PT. The anti-Stokes spectra show three peaks (-23, -18, and -13 cm^{-1}) from PMN-0.24PT and four peaks (-23, -18, -16, and -13 cm^{-1}) from PMN-0.33PT. All peaks are derived from the elastic vibrations by nanocluster itself, which correspond to torsional and spheroidal modes of

#212614 - $15.00 USD Received 23 May 2014; revised 18 Aug 2014; accepted 19 Aug 2014; published 2 Sep 2014

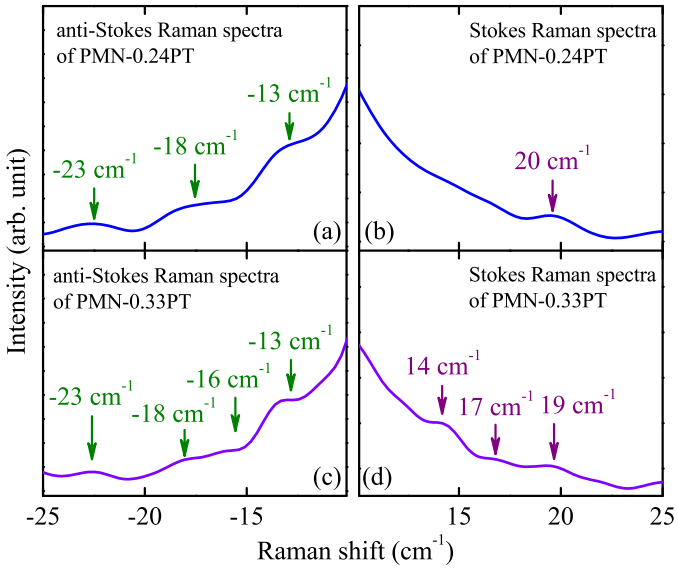

Fig. 2. (a) Anti-Stokes and (b) Stokes Raman spectra for PMN-0.24PT crystal. (c) Anti-Stokes and (d) Stokes Raman spectra of PMN-0.33PT crystal. Note that PMN-0.33PT crystal has more modes under both Anti-Stokes and Stokes configurations.

vibrations of spherical and/or ellipsoidal clusters [11]. These low wavenumber modes confirm polar nanoclusters in PMN-PT and indicate a hypothesis of the coreshell nanostructure with a 1 : 1 ordered negatively charged nanocore surrounded by a positively charged nanoshell [29]. The lower wavenumber modes (|wavenumber|<15 cm^{-1}) are derived from the outer interface, while the higher wavenumber modes (|wavenumber|> 15 cm^{-1}) arise from the inner interface [11]. Note that more LWRS modes appear in PMN-0.33PT, as compared to those in PMN-0.24PT. Number of these low wavenumber Raman modes is corresponding to the diversity of nanostructure size. Note that PMN-0.33PT is near MPB region with the coexistence of multiple phases. These multiple phases lead to a high disorder degree in the lattice. The distortion results in more peaks in both Stokes and anti-Stokes configurations because the phonon modes with particular frequency would be detected in nanostructures with the same size.

3.3. Polar nanoregions and structural variations

The above results imply that the PL emissions are sensitive to environmental changing in PMN-PT crystals. To further analyze temperature dependent phase transitions and nanostructures, the PL spectra should be well fitted. Figure 3 displays the experimental and best-fitting PL spectral data at 80 K for PMN-0.33PT crystal. Six emission peaks can be found as shown in Fig. 4. They are labeled as E_a, E_b, E_c, E_d, E_e, and E_f, in the order of decreasing photon energy, respectively. Note that two more peaks can be assigned between 1.5 to 2.5 eV when compared to bare spectra in Fig. 1 in order to increase degree of data point matching. The parameter E_a is from interband energy between bottom of the conduction band and top of the valence band as its energy is similar to bandgap energy of PMN-PT [15]. It shows two slope changes at 120 and 160 K (shaded regions in Fig. 4) with the rapid intensity decreasing from PMN-0.24PT and PMN-0.33PT crystals, respectively. The similar features are presented in emission peaks E_b, E_c, E_d, E_e, and E_f. These emissions are originated from bound states within the bandgap. They also show significant changes in low temperature regions. The correlation length of polar

#212614 - $15.00 USD Received 23 May 2014; revised 18 Aug 2014; accepted 19 Aug 2014; published 2 Sep 2014

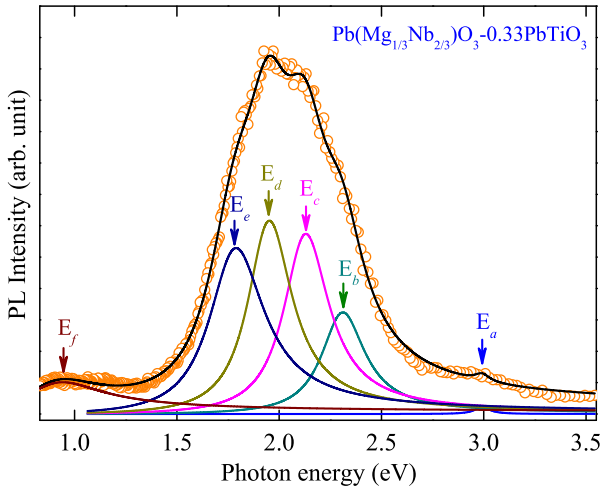

Fig. 3. Deconvolution of the PL spectra (solid line) for PMN-0.33PT crystal at 80 K (dotted line). The peak positions of six PL emissions are located at 2.99, 2.32, 2.14, 1.95, 1.80, and 0.93 eV, respectively. The letters a-f label these emissions in the order of decreasing the photon energy, respectively.

nanoclusters increases with decreasing temperature. The evolution of large size nanoclusters leads to the sudden change. Another powerful evidence can support the conclusion that the slope in low temperature region is larger in PMN-0.24PT than that in PMN-0.33PT. As we know, pure phase is conducive for the variation of polar nanoclusters while the multiphases in MPB region could weaken the evolution. This is consistent well with the variation in low temperature regions. Phase transitions also affect the PL emissions, especially the lower energy emissions E_d, E_e, and E_f. Transition from MPB to the T (tetragonal) phase (MPB-T phase transition) and transition from the T phase to C (cubic) phase (T-C phase transition) are relatively easier to be detected by PL spectra with distinct discontinuous at each phase transition temperature (dashed lines in Fig. 4). Discernable decline of E_a and E_c and jumps of E_d, E_e, and E_f can be ascribed to the MPB-T phase transition at 240 K. An increasing step of E_a and E_c and a decreasing step of E_d, E_e, and E_f are observed at T-C phase transition temperature (300 K). The R-C (rhombohedral-cubic) phase transition can be identified from an increasing trend to constant of E_b and E_d in Fig. 4(c) and 4(g). Note that the intermediate phase (monoclinic) in PMN-0.24PT, which is sensitive to intensity of PL spectra, does not lead to significant changes in these emissions except for E_d.

These emissions are modulated by structure transformation, including not only phase transitions but also nanostructure evolution. It has been widely accepted that PNRs can drive the ferroelectricity [12]. The driven process can be divided into two steps with increasing temperature: (1) Scattered and large nanostructures combined into PNRs. Different symmetries of nanostructures lead to different surface charges. These charges initiate selective combination and form polar nanoclusters. (2) When the fraction of these clusters with different symmetries reached a critical point, macroscopic phase transitions are driven. The variations below 200 K indicate the process in step one. Temperature dependent Raman spectra and XRD patterns in $Pb(In_{1/2}Nb_{1/2})O_3$-$Pb(Mg_{1/3}Nb_{2/3})O_3$-$PbTiO_3$ crystals reveal the multiphase coexistences at 200 K [16]. The multiphase is essentially composed of nanoclusters with different symmetries. It confirms a powerful testifying of PL spectra in characterizing phase transitions.

Generally, polar nanoclusters should dissolve above the Burns temperature ($T_b \sim 550$ K) in

#212614 - $15.00 USD Received 23 May 2014; revised 18 Aug 2014; accepted 19 Aug 2014; published 2 Sep 2014

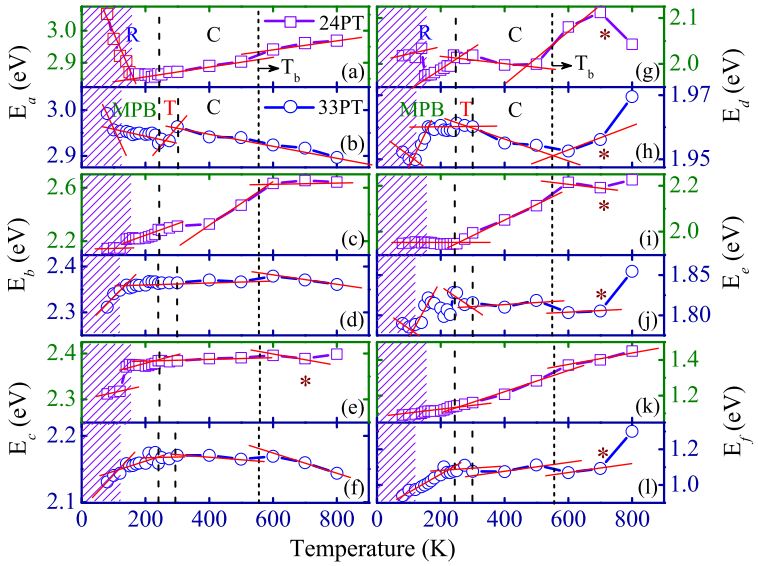

Fig. 4. Temperature dependence of well-fitted PL emissions E_a, E_b, E_c, E_d, E_e, and E_f for (a), (c), (e), (g), (i), (k) PMN-0.24PT crystal and (b), (d), (f), (h), (j), (l) PMN-0.33PT crystal, respectively. Note that the symbol "$*$" marks the inflection point at 700 K and the solid lines are guides for eyes. The shaded parts indicate low temperature phase (R or MPB) regions.

PMN-PT and its related systems [12, 30]. That means the PL emissions should remain constant or show a linear behavior above T_b, where only pure phase (C phase) exists without nanostructure. However, significant inflection points in E_d, E_e, and E_f are found at 700 K from both PMN-0.24PT and PMN-0.33PT. It indicates the core-shell nanostructure with more thermal stability. This nanostructure is formed with a 1 : 1 ordered negatively charged nanocore surrounded by a positively charged nanoshell, which was proposed previously in this related systems [11]. It is reasonable to infer that the core-shell nanostructure leads to these inflection points at 700 K because the core-shell nanostructure can resist higher temperature and exist even above T_b.

3.4. Thermal quenching of PL emissions

Thermal quenching of PL emissions is usually found in Nb-doped ABO_3 relaxor ferroelectrics, which is attributed to the recombination through a non-radiative channel or the polar nanoclusters. The observation of peak b in Fig. 1 has a strong resemblance with thermal quenching reported in Nb-doped $BaTiO_3$ and pure PMN [11, 31]. The expression for thermal quenching can be written as:

$$I = \frac{1}{A + B\exp(-E_{tq}/kT)}. \tag{2}$$

Here, I is the intensity of PL spectra. T is the temperature and k is Boltzmann constant. A and B are constants [32]. The above expression gives an activation energy (E_{tq}) of 143 meV (1154 cm^{-1}) for pure PMN polycrystalline [20]. To confirm the phonon presence in PMN-PT single crystal, Raman scattering measurements have been carried out. As can be seen in Fig. 5, a mode at about 141.9 meV (1145 cm^{-1}) can be clearly observed. The slight difference of the activation energy between PMN and PMN-PT is due to different lattice with the introduction of Ti. Nevertheless, the mode is very weak, which indicates that it is a defect-induced Raman

#212614 - $15.00 USD Received 23 May 2014; revised 18 Aug 2014; accepted 19 Aug 2014; published 2 Sep 2014

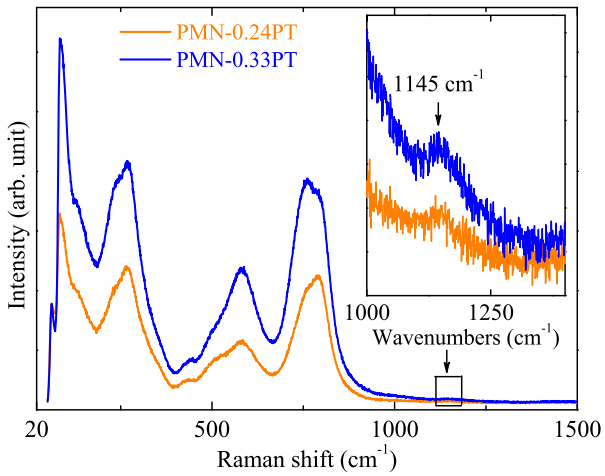

Fig. 5. Raman spectra for PMN-0.24PT and PMN-0.33PT crystals recorded at room temperature. The inset shows an enlarged region near the phonon mode of 1145 cm^{-1}.

mode in the polar nanoclusters. This recombination through a non-radiative channel leads to thermal quenching of emission peak b in PMN-PT single crystals.

4. Conclusions

In summary, temperature and composition dependences of interband emissions and nanostructure of PMN-PT single crystals have been investigated using PL spectral measurement and low-wavenumber Raman scattering. Discontinuous evolution of position and intensity from PL emissions can be clearly identified and attributed to phase transitions and dissolving of polar nanostructures in PMN-PT. The Raman mode of 1145 cm^{-1} indicates that PL phenomenon can be modulated by thermal quenching.

Acknowledgments

This work was financially supported by Major State Basic Research Development Program of China (Grant Nos. 2011CB922200 and 2013CB922300), Natural Science Foundation of China (Grant Nos. 11374097 and 61376129), Projects of Science and Technology Commission of Shanghai Municipality (Grant Nos. 14XD1401500, 13JC1402100 and 13JC1404200), and the Program for Professor of Special Appointment (Eastern Scholar) at Shanghai Institutions of Higher Learning.

#212614 - $15.00 USD Received 23 May 2014; revised 18 Aug 2014; accepted 19 Aug 2014; published 2 Sep 2014